Dalitz plot analysis of $D_s^+ \to \pi^+\pi^-\pi^+$

B. Aubert,[1] M. Bona,[1] Y. Karyotakis,[1] J. P. Lees,[1] V. Poireau,[1] E. Prencipe,[1] X. Prudent,[1] V. Tisserand,[1] J. Garra Tico,[2] E. Grauges,[2] L. Lopez,[3a,3b] A. Palano,[3a,3b] M. Pappagallo,[3a,3b] G. Eigen,[4] B. Stugu,[4] L. Sun,[4] G. S. Abrams,[5] M. Battaglia,[5] D. N. Brown,[5] R. G. Jacobsen,[5] L. T. Kerth,[5] Yu. G. Kolomensky,[5] G. Lynch,[5] I. L. Osipenkov,[5] M. T. Ronan,[5,*] K. Tackmann,[5] T. Tanabe,[5] C. M. Hawkes,[6] N. Soni,[6] A. T. Watson,[6] H. Koch,[7] T. Schroeder,[7] D. J. Asgeirsson,[8] B. G. Fulsom,[8] C. Hearty,[8] T. S. Mattison,[8] J. A. McKenna,[8] M. Barrett,[9] A. Khan,[9] V. E. Blinov,[10] A. D. Bukin,[10] A. R. Buzykaev,[10] V. P. Druzhinin,[10] V. B. Golubev,[10] A. P. Onuchin,[10] S. I. Serednyakov,[10] Yu. I. Skovpen,[10] E. P. Solodov,[10] K. Yu. Todyshev,[10] M. Bondioli,[11] S. Curry,[11] I. Eschrich,[11] D. Kirkby,[11] A. J. Lankford,[11] P. Lund,[11] M. Mandelkern,[11] E. C. Martin,[11] D. P. Stoker,[11] S. Abachi,[12] C. Buchanan,[12] H. Atmacan,[13] J. W. Gary,[13] F. Liu,[13] O. Long,[13] G. M. Vitug,[13] Z. Yasin,[13] L. Zhang,[13] V. Sharma,[14] C. Campagnari,[15] T. M. Hong,[15] D. Kovalskyi,[15] M. A. Mazur,[15] J. D. Richman,[15] T. W. Beck,[16] A. M. Eisner,[16] C. J. Flacco,[16] C. A. Heusch,[16] J. Kroseberg,[16] W. S. Lockman,[16] A. J. Martinez,[16] T. Schalk,[16] B. A. Schumm,[16] A. Seiden,[16] M. G. Wilson,[16] L. O. Winstrom,[16] C. H. Cheng,[17] D. A. Doll,[17] B. Echenard,[17] F. Fang,[17] D. G. Hitlin,[17] I. Narsky,[17] T. Piatenko,[17] F. C. Porter,[17] R. Andreassen,[18] G. Mancinelli,[18] B. T. Meadows,[18] K. Mishra,[18] M. D. Sokoloff,[18] P. C. Bloom,[19] W. T. Ford,[19] A. Gaz,[19] J. F. Hirschauer,[19] M. Nagel,[19] U. Nauenberg,[19] J. G. Smith,[19] S. R. Wagner,[19] R. Ayad,[20,†] A. Soffer,[20,‡] W. H. Toki,[20] R. J. Wilson,[20] E. Feltresi,[21] A. Hauke,[21] H. Jasper,[21] M. Karbach,[21] J. Merkel,[21] A. Petzold,[21] B. Spaan,[21] K. Wacker,[21] M. J. Kobel,[22] R. Nogowski,[22] K. R. Schubert,[22] R. Schwierz,[22] A. Volk,[22] D. Bernard,[23] G. R. Bonneaud,[23] E. Latour,[23] M. Verderi,[23] P. J. Clark,[24] S. Playfer,[24] J. E. Watson,[24] M. Andreotti,[25a,25b] D. Bettoni,[25a] C. Bozzi,[25a] R. Calabrese,[25a,25b] A. Cecchi,[25a,25b] G. Cibinetto,[25a,25b] P. Franchini,[25a,25b] E. Luppi,[25a,25b] M. Negrini,[25a,25b] A. Petrella,[25a,25b] L. Piemontese,[25a] V. Santoro,[25a,25b] R. Baldini-Ferroli,[26] A. Calcaterra,[26] R. de Sangro,[26] G. Finocchiaro,[26] S. Pacetti,[26] P. Patteri,[26] I. M. Peruzzi,[26,§] M. Piccolo,[26] M. Rama,[26] A. Zallo,[26] A. Buzzo,[27a] R. Contri,[27a,27b] M. Lo Vetere,[27a,27b] M. M. Macri,[27a] M. R. Monge,[27a,27b] S. Passaggio,[27a] C. Patrignani,[27a,27b] E. Robutti,[27a] A. Santroni,[27a,27b] S. Tosi,[27a,27b] K. S. Chaisanguanthum,[28] M. Morii,[28] A. Adametz,[29] J. Marks,[29] S. Schenk,[29] U. Uwer,[29] F. U. Bernlochner,[30] V. Klose,[30] H. M. Lacker,[30] D. J. Bard,[31] P. D. Dauncey,[31] M. Tibbetts,[31] P. K. Behera,[32] X. Chai,[32] M. J. Charles,[32] U. Mallik,[32] J. Cochran,[33] H. B. Crawley,[33] L. Dong,[33] W. T. Meyer,[33] S. Prell,[33] E. I. Rosenberg,[33] A. E. Rubin,[33] Y. Y. Gao,[34] A. V. Gritsan,[34] Z. J. Guo,[34] C. K. Lae,[34] N. Arnaud,[35] J. Béquilleux,[35] A. D'Orazio,[35] M. Davier,[35] J. Firmino da Costa,[35] G. Grosdidier,[35] F. Le Diberder,[35] V. Lepeltier,[35] A. M. Lutz,[35] S. Pruvot,[35] P. Roudeau,[35] M. H. Schune,[35] J. Serrano,[35] V. Sordini,[35,‖] A. Stocchi,[35] G. Wormser,[35] D. J. Lange,[36] D. M. Wright,[36] I. Bingham,[37] J. P. Burke,[37] C. A. Chavez,[37] J. R. Fry,[37] E. Gabathuler,[37] R. Gamet,[37] D. E. Hutchcroft,[37] D. J. Payne,[37] C. Touramanis,[37] A. J. Bevan,[38] C. K. Clarke,[38] F. Di Lodovico,[38] R. Sacco,[38] M. Sigamani,[38] G. Cowan,[39] S. Paramesvaran,[39] A. C. Wren,[39] D. N. Brown,[40] C. L. Davis,[40] A. G. Denig,[41] M. Fritsch,[41] W. Gradl,[41] K. E. Alwyn,[42] D. Bailey,[42] R. J. Barlow,[42] G. Jackson,[42] G. D. Lafferty,[42] T. J. West,[42] J. I. Yi,[42] J. Anderson,[43] C. Chen,[43] A. Jawahery,[43] D. A. Roberts,[43] G. Simi,[43] J. M. Tuggle,[43] C. Dallapiccola,[44] X. Li,[44] E. Salvati,[44] S. Saremi,[44] R. Cowan,[45] D. Dujmic,[45] P. H. Fisher,[45] S. W. Henderson,[45] G. Sciolla,[45] M. Spitznagel,[45] F. Taylor,[45] R. K. Yamamoto,[45] M. Zhao,[45] P. M. Patel,[46] S. H. Robertson,[46] A. Lazzaro,[47a,47b] V. Lombardo,[47a] F. Palombo,[47a,47b] J. M. Bauer,[48] L. Cremaldi,[48] R. Godang,[48,¶] R. Kroeger,[48] D. J. Summers,[48] H. W. Zhao,[48] M. Simard,[49] P. Taras,[49] H. Nicholson,[50] G. De Nardo,[51a,51b] L. Lista,[51a] D. Monorchio,[51a,51b] G. Onorato,[51a,51b] C. Sciacca,[51a,51b] G. Raven,[52] H. L. Snoek,[52] C. P. Jessop,[53] K. J. Knoepfel,[53] J. M. LoSecco,[53] W. F. Wang,[53] L. A. Corwin,[54] K. Honscheid,[54] H. Kagan,[54] R. Kass,[54] J. P. Morris,[54] A. M. Rahimi,[54] J. J. Regensburger,[54] S. J. Sekula,[54] Q. K. Wong,[54] N. L. Blount,[55] J. Brau,[55] R. Frey,[55] O. Igonkina,[55] J. A. Kolb,[55] M. Lu,[55] R. Rahmat,[55] N. B. Sinev,[55] D. Strom,[55] J. Strube,[55] E. Torrence,[55] G. Castelli,[56a,56b] N. Gagliardi,[56a,56b] M. Margoni,[56a,56b] M. Morandin,[56a] M. Posocco,[56a] M. Rotondo,[56a] F. Simonetto,[56a,56b] R. Stroili,[56a,56b] C. Voci,[56a,56b] P. del Amo Sanchez,[57] E. Ben-Haim,[57] H. Briand,[57] G. Calderini,[57] J. Chauveau,[57] O. Hamon,[57] Ph. Leruste,[57] J. Ocariz,[57] A. Perez,[57] J. Prendki,[57] S. Sitt,[57] L. Gladney,[58] M. Biasini,[59a,59b] E. Manoni,[59a,59b] C. Angelini,[60a,60b] G. Batignani,[60a,60b] S. Bettarini,[60a,60b] M. Carpinelli,[60a,60b,**] A. Cervelli,[60a,60b] F. Forti,[60a,60b] M. A. Giorgi,[60a,60b] A. Lusiani,[60a,60c] G. Marchiori,[60a,60b] M. Morganti,[60a,60b] N. Neri,[60a,60b] E. Paoloni,[60a,60b] G. Rizzo,[60a,60b] J. J. Walsh,[60a] D. Lopes Pegna,[61] C. Lu,[61] J. Olsen,[61] A. J. S. Smith,[61] A. V. Telnov,[61] F. Anulli,[62a] E. Baracchini,[62a,62b] G. Cavoto,[62a] R. Faccini,[62a,62b] F. Ferrarotto,[62a] F. Ferroni,[62a,62b] M. Gaspero,[62a,62b] P. D. Jackson,[62a] L. Li Gioi,[62a] M. A. Mazzoni,[62a] S. Morganti,[62a] G. Piredda,[62a] F. Renga,[62a,62b] C. Voena,[62a] M. Ebert,[63] T. Hartmann,[63] H. Schröder,[63] R. Waldi,[63] T. Adye,[64] B. Franek,[64] E. O. Olaiya,[64] F. F. Wilson,[64] S. Emery,[65] M. Escalier,[65] L. Esteve,[65] G. Hamel de Monchenault,[65] W. Kozanecki,[65] G. Vasseur,[65] Ch. Yèche,[65] M. Zito,[65] X. R. Chen,[66] H. Liu,[66] W. Park,[66] M. V. Purohit,[66] R. M. White,[66] J. R. Wilson,[66]

M. T. Allen,[67] D. Aston,[67] R. Bartoldus,[67] J. F. Benitez,[67] R. Cenci,[67] J. P. Coleman,[67] M. R. Convery,[67] J. C. Dingfelder,[67] J. Dorfan,[67] G. P. Dubois-Felsmann,[67] W. Dunwoodie,[67] R. C. Field,[67] A. M. Gabareen,[67] M. T. Graham,[67] P. Grenier,[67] C. Hast,[67] W. R. Innes,[67] J. Kaminski,[67] M. H. Kelsey,[67] H. Kim,[67] P. Kim,[67] M. L. Kocian,[67] D. W. G. S. Leith,[67] S. Li,[67] B. Lindquist,[67] S. Luitz,[67] V. Luth,[67] H. L. Lynch,[67] D. B. MacFarlane,[67] H. Marsiske,[67] R. Messner,[67] D. R. Muller,[67] H. Neal,[67] S. Nelson,[67] C. P. O'Grady,[67] I. Ofte,[67] M. Perl,[67] B. N. Ratcliff,[67] A. Roodman,[67] A. A. Salnikov,[67] R. H. Schindler,[67] J. Schwiening,[67] A. Snyder,[67] D. Su,[67] M. K. Sullivan,[67] K. Suzuki,[67] S. K. Swain,[67] J. M. Thompson,[67] J. Va'vra,[67] A. P. Wagner,[67] M. Weaver,[67] C. A. West,[67] W. J. Wisniewski,[67] M. Wittgen,[67] D. H. Wright,[67] H. W. Wulsin,[67] A. K. Yarritu,[67] K. Yi,[67] C. C. Young,[67] V. Ziegler,[67] P. R. Burchat,[68] A. J. Edwards,[68] T. S. Miyashita,[68] S. Ahmed,[69] M. S. Alam,[69] J. A. Ernst,[69] B. Pan,[69] M. A. Saeed,[69] S. B. Zain,[69] S. M. Spanier,[70] B. J. Wogsland,[70] R. Eckmann,[71] J. L. Ritchie,[71] A. M. Ruland,[71] C. J. Schilling,[71] R. F. Schwitters,[71] B. W. Drummond,[72] J. M. Izen,[72] X. C. Lou,[72] F. Bianchi,[73a,73b] D. Gamba,[73a,73b] M. Pelliccioni,[73a,73b] M. Bomben,[74a,74b] L. Bosisio,[74a,74b] C. Cartaro,[74a,74b] G. Della Ricca,[74a,74b] L. Lanceri,[74a,74b] L. Vitale,[74a,74b] V. Azzolini,[75] N. Lopez-March,[75] F. Martinez-Vidal,[75] D. A. Milanes,[75] A. Oyanguren,[75] J. Albert,[76] Sw. Banerjee,[76] B. Bhuyan,[76] H. H. F. Choi,[76] K. Hamano,[76] R. Kowalewski,[76] M. J. Lewczuk,[76] I. M. Nugent,[76] J. M. Roney,[76] R. J. Sobie,[76] T. J. Gershon,[77] P. F. Harrison,[77] J. Ilic,[77] T. E. Latham,[77] G. B. Mohanty,[77] M. R. Pennington,[77,††] H. R. Band,[78] X. Chen,[78] S. Dasu,[78] K. T. Flood,[78] Y. Pan,[78] R. Prepost,[78] C. O. Vuosalo,[78] and S. L. Wu[78]

(*BABAR* Collaboration)

[1]*Laboratoire de Physique des Particules, IN2P3/CNRS et Université de Savoie, F-74941 Annecy-Le-Vieux, France*
[2]*Universitat de Barcelona, Facultat de Fisica, Departament ECM, E-08028 Barcelona, Spain*
[3a]*INFN Sezione di Bari, I-70126 Bari, Italy*
[3b]*Dipartmento di Fisica, Università di Bari, I-70126 Bari, Italy*
[4]*University of Bergen, Institute of Physics, N-5007 Bergen, Norway*
[5]*Lawrence Berkeley National Laboratory and University of California, Berkeley, California 94720, USA*
[6]*University of Birmingham, Birmingham, B15 2TT, United Kingdom*
[7]*Ruhr Universität Bochum, Institut für Experimentalphysik 1, D-44780 Bochum, Germany*
[8]*University of British Columbia, Vancouver, British Columbia, Canada V6T 1Z1*
[9]*Brunel University, Uxbridge, Middlesex UB8 3PH, United Kingdom*
[10]*Budker Institute of Nuclear Physics, Novosibirsk 630090, Russia*
[11]*University of California at Irvine, Irvine, California 92697, USA*
[12]*University of California at Los Angeles, Los Angeles, California 90024, USA*
[13]*University of California at Riverside, Riverside, California 92521, USA*
[14]*University of California at San Diego, La Jolla, California 92093, USA*
[15]*University of California at Santa Barbara, Santa Barbara, California 93106, USA*
[16]*University of California at Santa Cruz, Institute for Particle Physics, Santa Cruz, California 95064, USA*
[17]*California Institute of Technology, Pasadena, California 91125, USA*
[18]*University of Cincinnati, Cincinnati, Ohio 45221, USA*
[19]*University of Colorado, Boulder, Colorado 80309, USA*
[20]*Colorado State University, Fort Collins, Colorado 80523, USA*
[21]*Technische Universität Dortmund, Fakultät Physik, D-44221 Dortmund, Germany*
[22]*Technische Universität Dresden, Institut für Kernund Teilchenphysik, D-01062 Dresden, Germany*
[23]*Laboratoire Leprince-Ringuet, CNRS/IN2P3, Ecole Polytechnique, F-91128 Palaiseau, France*
[24]*University of Edinburgh, Edinburgh EH9 3JZ, United Kingdom*
[25a]*INFN Sezione di Ferrara, I-44100 Ferrara, Italy*
[25b]*Dipartimento di Fisica, Università di Ferrara, I-44100 Ferrara, Italy*
[26]*INFN Laboratori Nazionali di Frascati, I-00044 Frascati, Italy*
[27a]*INFN Sezione di Genova, I-16146 Genova, Italy*
[27b]*Dipartimento di Fisica, Università di Genova, I-16146 Genova, Italy*
[28]*Harvard University, Cambridge, Massachusetts 02138, USA*
[29]*Universität Heidelberg, Physikalisches Institut, Philosophenweg 12, D-69120 Heidelberg, Germany*
[30]*Humboldt-Universität zu Berlin, Institut für Physik, Newtonstr. 15, D-12489 Berlin, Germany*
[31]*Imperial College London, London, SW7 2AZ, United Kingdom*
[32]*University of Iowa, Iowa City, Iowa 52242, USA*
[33]*Iowa State University, Ames, Iowa 50011-3160, USA*
[34]*Johns Hopkins University, Baltimore, Maryland 21218, USA*

[35]*Laboratoire de l'Accélérateur Linéaire, IN2P3/CNRS et Université Paris-Sud 11, Centre Scientifique d'Orsay, B. P. 34, F-91898 Orsay Cedex, France*
[36]*Lawrence Livermore National Laboratory, Livermore, California 94550, USA*
[37]*University of Liverpool, Liverpool L69 7ZE, United Kingdom*
[38]*Queen Mary, University of London, London, E1 4NS, United Kingdom*
[39]*University of London, Royal Holloway and Bedford New College, Egham, Surrey TW20 0EX, United Kingdom*
[40]*University of Louisville, Louisville, Kentucky 40292, USA*
[41]*Johannes Gutenberg-Universität Mainz, Institut für Kernphysik, D-55099 Mainz, Germany*
[42]*University of Manchester, Manchester M13 9PL, United Kingdom*
[43]*University of Maryland, College Park, Maryland 20742, USA*
[44]*University of Massachusetts, Amherst, Massachusetts 01003, USA*
[45]*Massachusetts Institute of Technology, Laboratory for Nuclear Science, Cambridge, Massachusetts 02139, USA*
[46]*McGill University, Montréal, Québec, Canada H3A 2T8*
[47a]*INFN Sezione di Milano, I-20133 Milano, Italy*
[47b]*Dipartimento di Fisica, Università di Milano, I-20133 Milano, Italy*
[48]*University of Mississippi, University, Mississippi 38677, USA*
[49]*Université de Montréal, Physique des Particules, Montréal, Québec, Canada H3C 3J7*
[50]*Mount Holyoke College, South Hadley, Massachusetts 01075, USA*
[51a]*INFN Sezione di Napoli, I-80126 Napoli, Italy*
[51b]*Dipartimento di Scienze Fisiche, Università di Napoli Federico II, I-80126 Napoli, Italy*
[52]*NIKHEF, National Institute for Nuclear Physics and High Energy Physics, NL-1009 DB Amsterdam, The Netherlands*
[53]*University of Notre Dame, Notre Dame, Indiana 46556, USA*
[54]*Ohio State University, Columbus, Ohio 43210, USA*
[55]*University of Oregon, Eugene, Oregon 97403, USA*
[56a]*INFN Sezione di Padova, I-35131 Padova, Italy*
[56b]*Dipartimento di Fisica, Università di Padova, I-35131 Padova, Italy*
[57]*Laboratoire de Physique Nucléaire et de Hautes Energies, IN2P3/CNRS, Université Pierre et Marie Curie-Paris6, Université Denis Diderot-Paris7, F-75252 Paris, France*
[58]*University of Pennsylvania, Philadelphia, Pennsylvania 19104, USA*
[59a]*INFN Sezione di Perugia, I-06100 Perugia, Italy*
[59b]*Dipartimento di Fisica, Università di Perugia, I-06100 Perugia, Italy*
[60a]*INFN Sezione di Pisa, I-56127 Pisa, Italy*
[60b]*Dipartimento di Fisica, Università di Pisa, I-56127 Pisa, Italy*
[60c]*Scuola Normale Superiore di Pisa, I-56127 Pisa, Italy*
[61]*Princeton University, Princeton, New Jersey 08544, USA*
[62a]*INFN Sezione di Roma, I-00185 Roma, Italy*
[62b]*Dipartimento di Fisica, Università di Roma La Sapienza, I-00185 Roma, Italy*
[63]*Universität Rostock, D-18051 Rostock, Germany*
[64]*Rutherford Appleton Laboratory, Chilton, Didcot, Oxon, OX11 0QX, United Kingdom*
[65]*CEA, Irfu, SPP, Centre de Saclay, F-91191 Gif-sur-Yvette, France*
[66]*University of South Carolina, Columbia, South Carolina 29208, USA*
[67]*Stanford Linear Accelerator Center, Stanford, California 94309, USA*
[68]*Stanford University, Stanford, California 94305-4060, USA*
[69]*State University of New York, Albany, New York 12222, USA*
[70]*University of Tennessee, Knoxville, Tennessee 37996, USA*
[71]*University of Texas at Austin, Austin, Texas 78712, USA*
[72]*University of Texas at Dallas, Richardson, Texas 75083, USA*
[73a]*INFN Sezione di Torino, I-10125 Torino, Italy*
[73b]*Dipartimento di Fisica Sperimentale, Università di Torino, I-10125 Torino, Italy*
[74a]*INFN Sezione di Trieste, I-34127 Trieste, Italy*

[*]Deceased.
[†]Now at Temple University, Philadelphia, PA 19122, USA.
[‡]Now at Tel Aviv University, Tel Aviv, 69978, Israel.
[§]Also with Università di Perugia, Dipartimento di Fisica, Perugia, Italy.
[‖]Also with Università di Roma La Sapienza, I-00185 Roma, Italy.
[¶]Now at University of South Alabama, Mobile, AL 36688, USA.
[**]Also with Università di Sassari, Sassari, Italy.
[††]Also with Institute for Particle Physics Phenomenology, Durham University, Durham DH1 3LE, United Kingdom.

[74b]*Dipartimento di Fisica, Università di Trieste, I-34127 Trieste, Italy*
[75]*IFIC, Universitat de Valencia-CSIC, E-46071 Valencia, Spain*
[76]*University of Victoria, Victoria, British Columbia, Canada V8W 3P6*
[77]*Department of Physics, University of Warwick, Coventry CV4 7AL, United Kingdom*
[78]*University of Wisconsin, Madison, Wisconsin 53706, USA*
(Received 9 December 2008; published 9 February 2009)

A Dalitz plot analysis of approximately 13 000 D_s^+ decays to $\pi^+\pi^-\pi^+$ has been performed. The analysis uses a 384 fb^{-1} data sample recorded by the *BABAR* detector at the PEP-II asymmetric-energy e^+e^- storage ring running at center of mass energies near 10.6 GeV. Amplitudes and phases of the intermediate resonances which contribute to this final state are measured. A high precision measurement of the ratio of branching fractions is performed: $\mathcal{B}(D_s^+ \to \pi^+\pi^-\pi^+)/\mathcal{B}(D_s^+ \to K^+K^-\pi^+) = 0.199 \pm 0.004 \pm 0.009$. Using a model-independent partial wave analysis, the amplitude and phase of the $\mathcal{S}$ wave have been measured.

DOI: 10.1103/PhysRevD.79.032003 PACS numbers: 13.20.Fc, 11.80.Et

I. INTRODUCTION

Dalitz plot analysis is an excellent way to study the dynamics of three-body charm decays. These decays are expected to proceed predominantly through intermediate quasi-two-body modes [1] and experimentally this is the observed pattern. Dalitz plot analyses can provide new information on the resonances that contribute to the observed three-body final states. In addition, since the intermediate quasi-two-body modes are dominated by light quark meson resonances, new information on light meson spectroscopy can be obtained.

Some puzzles still remain in light meson spectroscopy. There are new claims for the existence of broad states close to threshold such as $\kappa(800)$ and $f_0(600)$ [2]. The new evidence has reopened discussion of the composition of the ground state $J^{PC} = 0^{++}$ nonet, and of the possibility that states such as the $a_0(980)$ or $f_0(980)$ may be 4-quark states, due to their proximity to the $K\bar{K}$ threshold [3]. This hypothesis can be tested only through accurate measurements of the branching fractions and the couplings to different final states. It is therefore important to have precise information on the structure of the $\pi\pi$ $\mathcal{S}$ wave. In addition, comparison between the production of these states in decays of differently flavored charmed mesons $D^0(c\bar{u})$, $D^+(c\bar{d})$ and $D_s^+(c\bar{s})$ can yield new information on their possible quark composition. In this context, D_s^+ mesons can give information on the structure of the scalar amplitude coupled to $s\bar{s}$. Another benefit of studying charm decays is that, in some cases, partial wave analyses are able to isolate the scalar contribution with almost no background.

This paper focuses on the study of the three-body D_s^+ meson decays to $\pi^+\pi^-\pi^+$ [4] and performs, for the first time, a model-independent partial wave analysis (MIPWA) [5]. Previous Dalitz plot analyses of this decay mode were based on much smaller data samples [6,7] and did not have sufficient statistics to perform the detailed analysis reported here.

This paper is organized as follows. Section II briefly describes the *BABAR* detector, while Sec. III gives details on event reconstruction. Section IV is devoted to the evaluation of the selection efficiency. Section V deals with the Dalitz plot analysis of $D_s^+ \to \pi^+\pi^-\pi^+$ and results are given in Sec. VI. The measurement of the D_s^+ branching fraction is described in Sec. VII.

II. THE *BABAR* DETECTOR AND DATA SET

This analysis is based on data collected with the *BABAR* detector at the PEP-II asymmetric-energy e^+e^- collider at Stanford Linear Accelerator Center (SLAC). The data sample used in this analysis corresponds to an integrated luminosity of 347.5 fb^{-1} recorded at the $\Upsilon(4S)$ resonance (on-peak) and 36.5 fb^{-1} collected 40 MeV below the resonance (off-peak). The *BABAR* detector is described in detail elsewhere [8]. The following is a brief summary of the components important to this analysis. Charged particles are detected and their momenta measured by a combination of a cylindrical drift chamber (DCH) and a silicon vertex tracker (SVT), both operating within a 1.5 T solenoidal magnetic field. A ring-imaging Cherenkov detector (DIRC) is used for charged-particle identification. Photon energies are measured with a CsI electromagnetic calorimeter (EMC). Information from the DIRC and energy-loss measurements in the DCH and SVT are used to identify charged kaon and pion candidates. Monte Carlo (MC) events used in this analysis, $e^+e^- \to c\bar{c}$, are generated using the JETSET program [9], and the generated particles are propagated through a model of the *BABAR* detector with the GEANT4 simulation package [10]. Radiative corrections for signal and background processes are simulated using PHOTOS [11].

III. EVENT SELECTION AND D_s^+ RECONSTRUCTION

Events corresponding to the three-body decay

$$D_s^+ \to \pi^+\pi^-\pi^+ \tag{1}$$

are reconstructed from the sample of events having at least three reconstructed charged tracks with a net charge of ± 1

and having a minimum transverse momentum of 0.1 GeV/c. Tracks from D_s^+ decays are identified as pions or kaons by the Cherenkov angle θ_c measured with the DIRC. The typical separation between pions and kaons varies from 8σ at 2 GeV/c to 2.5σ at 4 GeV/c, where σ is the average resolution on θ_c. Lower momentum kaons are identified with a combination of θ_c (for momenta down to 0.7 GeV/c) and measurements of ionization energy loss dE/dx in the DCH and SVT. The particle identification efficiency is $\approx 95\%$, while the misidentification rate for kaons is $\approx 5\%$. Photons are identified as EMC clusters that do not have a spatial match with a charged track and that have a minimum energy of 100 MeV. To reject background, the lateral energy is required to be less than 0.8. The three tracks are fitted to a common vertex, and the χ^2 fit probability (labeled P_1) must be greater than 0.1%. A separate kinematic fit which makes use of the D_s^+ mass constraint, to be used in the Dalitz plot analysis, is also performed. To help discriminate signal from background, an additional fit which uses the constraint that the three tracks originate from the e^+e^- luminous region (beam spot) is performed. We label the χ^2 probability of this fit as P_2, and it is expected to be large for background and small for D_s^+ signal events, since in general the latter will have a measurable flight distance.

The combinatorial background is reduced by requiring the D_s^+ to originate from the decay

$$D_s^*(2112)^+ \to D_s^+\gamma \tag{2}$$

using the mass difference $\Delta m = m(\pi^+\pi^-\pi^+\gamma) - m(\pi^+\pi^-\pi^+)$. We cannot reliably extract the $D_s^*(2112)^+$ characteristics using the 3π decay mode due to the large background below the signal peak. Therefore we use the decay

$$D_s^+ \to K^+K^-\pi^+, \tag{3}$$

which has a much larger signal to background ratio. Fitting the mass difference $\Delta m = m(K^+K^-\pi^+\gamma) - m(K^+K^-\pi^+)$ for this decay mode with a polynomial describing the background and a single Gaussian for the signal, we obtain a width $\sigma = 5.51 \pm 0.04$ MeV/c^2. Since the experimental resolution in Δm is similar for the two D_s^+ decay modes, we require the value of Δm for the $D_s^+ \to \pi^+\pi^-\pi^+$ mode to be within $\pm 2\sigma$ of the Review of Particle Physics [12] value of the $[D_s^*(2112)^+ - D_s^+]$ mass difference. At this stage the three-pion invariant mass signal region, defined between $(-2\sigma, 2\sigma)$, where σ is estimated by a Gaussian fit to the D_s^+ line shapes, has a purity [signal/(signal + background)] of 4.3%.

Each D_s^+ candidate is characterized by three variables: the center of mass momentum p^*, the difference in probability $P_1 - P_2$, and the signed decay distance d_{xy} between the D_s^+ decay vertex and the beam spot projected in the plane normal to the beam collision axis. The distributions for these variables for background are inferred from the $D_s^+ \to \pi^+\pi^-\pi^+$ invariant mass sidebands defined between $(-9\sigma, -5\sigma)$ and $(5\sigma, 9\sigma)$. Since these variables are (to a good approximation) independent of the decay mode, the distributions for the three-pion invariant mass signal are inferred from the $D_s^+ \to K^+K^-\pi^+$ decay. These normalized distributions are then combined in a likelihood ratio test. The cut on the likelihood ratio has been chosen in order to obtain the largest statistics with background small enough to perform a Dalitz plot analysis.

Many possible background sources are examined. A small background contribution due to the decay $D^{*+} \to \pi^+ D^0$, where $D^0 \to \pi^+\pi^-$, is addressed by removing

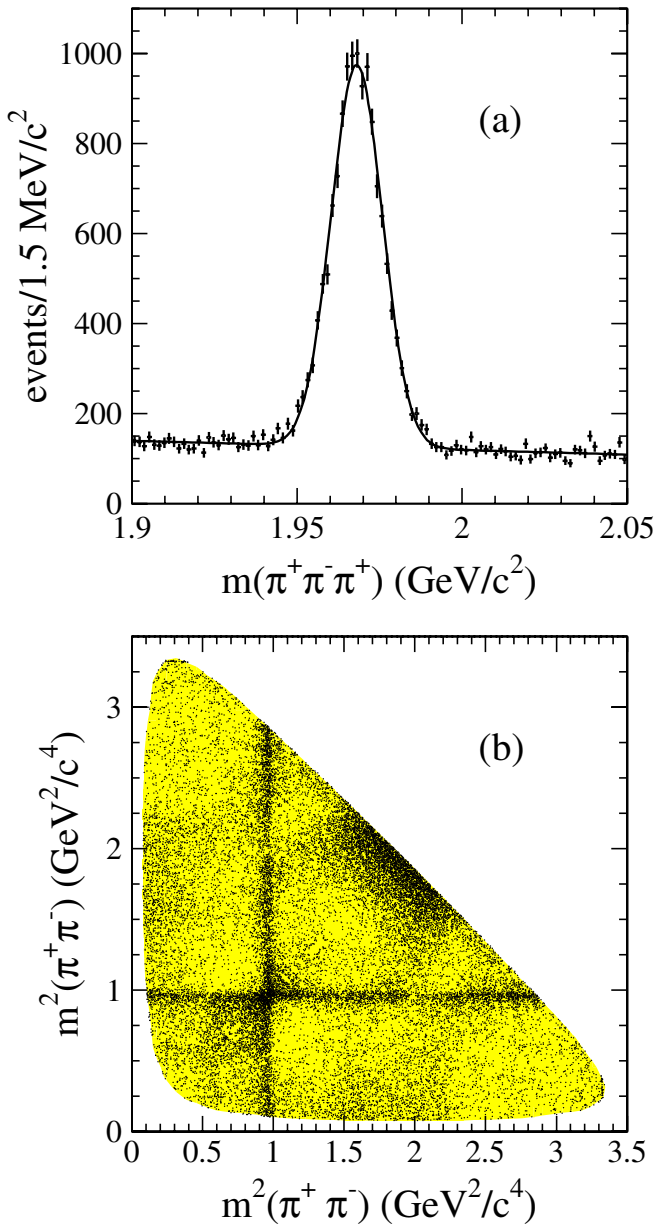

FIG. 1 (color online). (a) $\pi^+\pi^-\pi^+$ invariant mass distribution for the D_s^+ analysis sample. The line is the result of the fit described in the text. (b) Symmetrized $D_s^+ \to \pi^+\pi^-\pi^+$ Dalitz plot (two entries per event).

events with $|m(\pi^+\pi^-) - m_{D^0}| < 20.7$ MeV/c^2 and $m(\pi^+\pi^-\pi^+) - m(\pi^+\pi^-) < 0.1475$ GeV/c^2. Particle misidentification, in which a kaon ($K_{\rm mis}$) is wrongly identified as a pion, is tested by assigning the kaon mass to each pion in turn. In this way we observe a clean signal in the mass difference $m(\pi^+K^-_{\rm mis}\pi^+) - m(\pi^+K^-_{\rm mis})$ due to the decay $D^{*+} \to \pi^+ D^0$, where $D^0 \to K^-_{\rm mis}\pi^+$. Removing events with $|m(K^-_{\rm mis}\pi^+) - m_{D^0}| < 21.7$ MeV/c^2 and $m(\pi^+K^-_{\rm mis}\pi^+) - m(K^-_{\rm mis}\pi^+) < 0.1475$ GeV/c^2 diminishes this background. Finally, events having more than one candidate are removed from the sample (1.2% of the events).

The resulting $\pi^+\pi^-\pi^+$ mass distribution is shown in Fig. 1(a). This distribution has been fitted with a single Gaussian for the signal and a linear background function. The fit gives a D_s^+ mass of (1968.1 ± 0.1) MeV/c^2 and width $\sigma = 7.77 \pm 0.09$ MeV/c^2 (statistical error only). The signal region contains 13 179 events with a purity of 80%. The resulting Dalitz plot, symmetrized along the two axes, is shown in Fig. 1(b). For this distribution, and in the following Dalitz plot analysis, we use the track momenta obtained from the D_s^+ mass-constrained fit. We observe a clear $f_0(980)$ signal, evidenced by the two narrow crossing bands. We also observe a broad accumulation of events in the 1.9 GeV$^2/c^4$ region.

IV. EFFICIENCY

The efficiency for this D_s^+ decay mode is determined from a sample of Monte Carlo events in which the D_s^+ decay is generated according to phase space (i.e. such that the Dalitz plot is uniformly populated). These events are passed through a full detector simulation and subjected to the same reconstruction and event selection procedure applied to the data. The distribution of the selected events in the Dalitz plot is then used to determine the total reconstruction and selection efficiency. The MC sample $e^+e^- \to D_s^{*+}X$, where $D_s^{*+} \to \gamma D_s^+$, used to compute this efficiency consists of 27.4×10^6 generated events for $D_s^+ \to \pi^+\pi^-\pi^+$ and 4.2×10^6 for $D_s^+ \to K^+K^-\pi^+$. The Dalitz plot is divided into small cells and the efficiency distribution is fitted with a second-order polynomial in two dimensions. The efficiency is found to be almost uniform as a function of the $\pi^+\pi^-$ invariant mass with an average value of $\approx 1.6\%$. This low efficiency is mainly due to the likelihood ratio selection: it is 18.0% without this cut.

The experimental resolution as a function of the $\pi^+\pi^-$ mass has been computed as the difference between MC generated and reconstructed mass. It increases from 1.0 to 2.5 MeV/c^2 from the $\pi^+\pi^-$ threshold to 1.0 GeV/c^2.

V. DALITZ PLOT ANALYSIS

An unbinned maximum likelihood fit is performed on the distribution of events in the Dalitz plot to determine the relative amplitudes and phases of intermediate resonant and nonresonant states. The likelihood function is

$$\mathcal{L} = \prod_{\rm events}\Bigg[x(m)\cdot\eta(m_1^2,m_2^2)\frac{\sum_{i,j}c_ic_j^*A_iA_j^*}{\sum_{i,j}c_ic_j^*I_{A_iA_j^*}} + (1-x(m))\frac{\sum_i|k_i|^2B_i^2}{\sum_i|k_i|^2I_{B_i^2}}\Bigg], \quad (4)$$

where

(i) m_1^2 and m_2^2 are the squared $\pi^+\pi^-$ effective masses.

(ii) $x(m)$ is the mass-dependent fraction of signal, defined as $x(m) = \frac{G(m)}{G(m)+P(m)}$. Here $G(m)$ and $P(m)$ represent the Gaussian and the linear function used to fit the $\pi^+\pi^-\pi^+$ mass spectrum, respectively.

(iii) $\eta(m_1^2, m_2^2)$ is the efficiency, parametrized with a two-dimensional second-order polynomial.

(iv) A_i and B_i describe signal and background amplitude contributions, respectively.

(v) k_i are real factors describing the structure of background. They are computed by fitting the sideband regions.

(vi) $I_{A_iA_j^*} = \int A_iA_j^*\eta(m_1^2,m_2^2)dm_1^2dm_2^2$ and $I_{B_i^2}$ are the normalization integrals for signal and background, respectively. The products of efficiency and amplitudes are normalized using a numerical integration over the Dalitz plot.

(vii) c_i are complex coefficients allowed to vary during the fit procedure.

The efficiency-corrected fraction due to the resonant or nonresonant contribution i is defined as follows:

$$f_i = \frac{|c_i|^2\int|A_i|^2dm_1^2dm_2^2}{\sum_{j,k}c_jc_k^*\int A_jA_k^*dm_1^2dm_2^2}. \quad (5)$$

The f_i values do not necessarily add to 1 because of interference effects. The uncertainty on each f_i is evaluated by propagating the full covariance matrix obtained from the fit.

The phase of each amplitude (i.e. the phase of the corresponding c_i) is measured with respect to the $f_2(1270)\pi^+$ amplitude. Each $\mathcal{P}$ wave and $\mathcal{D}$ wave amplitude A_i is represented by the product of a complex Breit-Wigner function [BW(m)] and a real angular term:

$$A = {\rm BW}(m)\times T(\Omega), \quad (6)$$

where m is the $\pi^+\pi^-$ mass. The Breit-Wigner function includes the Blatt-Weisskopf form factors [13]. The angular terms $T(\Omega)$ are described in Ref. [12].

For the $\pi^+\pi^-$ $\mathcal{S}$ wave amplitude, we use a different approach because

(i) Scalar resonances have large uncertainties. In addition, the existence of some states needs confirmation.

(ii) Modeling the $\mathcal{S}$ wave as a superposition of Breit-Wigner functions is unphysical since it leads to a violation of unitarity when broad resonances overlap.

To overcome these problems, we use a model-independent partial wave analysis introduced by the Fermilab E791 Collaboration [5]: instead of including the $\mathcal{S}$ wave amplitude as a superposition of relativistic Breit-Wigner functions, we divide the $\pi^+\pi^-$ mass spectrum into 29 slices and we parametrize the $\mathcal{S}$ wave by an interpolation between the 30 end points in the complex plane:

$$A_{\mathcal{S}\text{ wave}}(m_{\pi\pi}) = \text{Interp}(c_k(m_{\pi\pi})e^{i\phi_k(m_{\pi\pi})})_{k=1,..,30}. \quad (7)$$

The amplitude and phase of each end point are free parameters. The width of each slice is tuned to get approximately the same number of $\pi^+\pi^-$ combinations ($\simeq 13\,179 \times 2/29$). Interpolation is implemented by a relaxed cubic spline [14]. The phase is not constrained in a specific range in order to allow the spline to be a continuous function.

The background shape is obtained by fitting the D_s^+ sidebands. In this fit, resonances are assumed to be incoherent, i.e. are represented by Breit-Wigner intensity terms only. A good representation of the background includes

TABLE I. Results from the $D_s^+ \to \pi^+\pi^-\pi^+$ Dalitz plot analysis. The table reports the fit fractions, amplitudes and phases. Errors are statistical and systematic, respectively.

Decay mode	Decay fraction (%)	Amplitude	Phase (rad)
$f_2(1270)\pi^+$	$10.1 \pm 1.5 \pm 1.1$	1.0 (fixed)	0.0 (fixed)
$\rho(770)\pi^+$	$1.8 \pm 0.5 \pm 1.0$	$0.19 \pm 0.02 \pm 0.12$	$1.1 \pm 0.1 \pm 0.2$
$\rho(1450)\pi^+$	$2.3 \pm 0.8 \pm 1.7$	$1.2 \pm 0.3 \pm 1.0$	$4.1 \pm 0.2 \pm 0.5$
$\mathcal{S}$ wave	$83.0 \pm 0.9 \pm 1.9$	Table II	Table II
Total	$97.2 \pm 3.7 \pm 3.8$		
χ^2/NDF	$\frac{437}{422-64} = 1.2$		

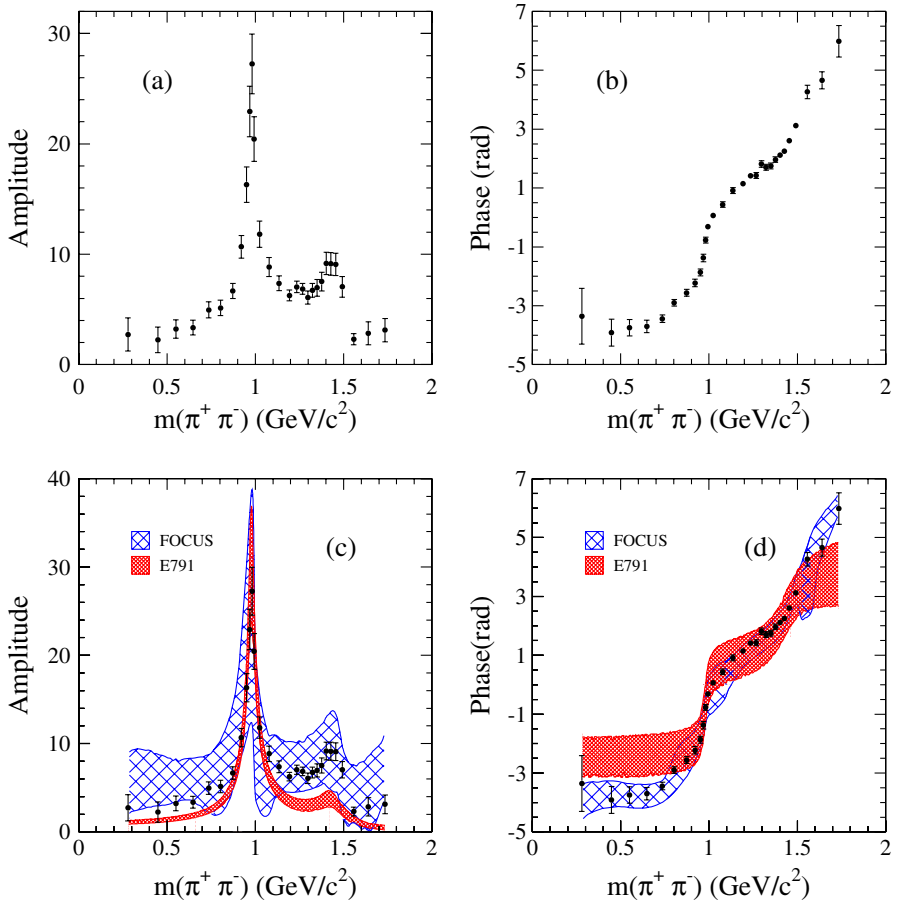

FIG. 2 (color online). (a) $\mathcal{S}$ wave amplitude extracted from the best fit, (b) corresponding $\mathcal{S}$ wave phase, (c) $\mathcal{S}$ wave amplitude compared to the FOCUS and E791 amplitudes, and (d) $\mathcal{S}$ wave phase compared to the FOCUS and E791 phases. Errors are statistical only.

contributions from K^0_S, $\rho^0(770)$ and three *ad hoc* scalar resonances with free parameters.

Resonances are included in sequence, keeping only those having a fractional significance greater than 2 standard deviations.

VI. RESULTS

The fit results (fractions and phases) are summarized in Table I. The resulting $\pi^+\pi^-$ $\mathcal{S}$ wave amplitude and phase is shown in Figs. 2(a) and 2(b) and is given numerically in Table II. Figures 2(c) and 2(d) show a comparison with the resulting $\mathcal{S}$ wave from the E791 experiment, which performed a Dalitz plot analysis using an isobar model [6], and the FOCUS experiment, which made use of the K-matrix formalism [7]. In the two figures, the two bands have been obtained by propagating the measurement errors and assuming no correlations. This assumption may influence the calculation of the uncertainties on the phases and amplitudes which are different in the two experiments.

The Dalitz plot projections together with the fit results are shown in Fig. 3. Here we label with $m^2(\pi^+\pi^-)_{\rm low}$ and $m^2(\pi^+\pi^-)_{\rm high}$ the lower and higher values, respectively, of the two $\pi^+\pi^-$ mass combinations.

TABLE II. Amplitude and phase of the $\pi^-\pi^+$ $\mathcal{S}$ wave amplitude determined with the MIPWA fit described in the text. The first error is statistical while the second is systematic.

Interval	Mass (GeV/c^2)	Amplitude	Phase (radians)
1	0.28	$2.7 \pm 1.5 \pm 2.4$	$-3.4 \pm 1.0 \pm 1.3$
2	0.448	$2.2 \pm 1.2 \pm 1.3$	$-3.9 \pm 0.5 \pm 0.4$
3	0.55	$3.2 \pm 0.8 \pm 1.1$	$-3.7 \pm 0.3 \pm 0.3$
4	0.647	$3.3 \pm 0.7 \pm 0.9$	$-3.7 \pm 0.2 \pm 0.3$
5	0.736	$5.0 \pm 0.7 \pm 1.1$	$-3.4 \pm 0.1 \pm 0.2$
6	0.803	$5.1 \pm 0.7 \pm 0.8$	$-2.9 \pm 0.1 \pm 0.2$
7	0.873	$6.7 \pm 0.7 \pm 0.7$	$-2.6 \pm 0.1 \pm 0.3$
8	0.921	$10.7 \pm 1.0 \pm 0.9$	$-2.2 \pm 0.1 \pm 0.2$
9	0.951	$16.3 \pm 1.6 \pm 1.2$	$-1.9 \pm 0.1 \pm 0.2$
10	0.968	$22.9 \pm 2.3 \pm 1.5$	$-1.4 \pm 0.1 \pm 0.1$
11	0.981	$27.2 \pm 2.7 \pm 1.6$	$-0.8 \pm 0.1 \pm 0.2$
12	0.993	$20.4 \pm 2.0 \pm 0.9$	$-0.3 \pm 0.1 \pm 0.2$
13	1.024	$11.8 \pm 1.2 \pm 0.5$	$0.1 \pm 0.1 \pm 0.2$
14	1.078	$8.8 \pm 0.9 \pm 0.3$	$0.4 \pm 0.1 \pm 0.1$
15	1.135	$7.4 \pm 0.7 \pm 0.3$	$0.9 \pm 0.1 \pm 0.1$
16	1.193	$6.3 \pm 0.5 \pm 0.2$	$1.1 \pm 0.1 \pm 0.1$
17	1.235	$7.0 \pm 0.5 \pm 0.3$	$1.4 \pm 0.1 \pm 0.1$
18	1.267	$6.9 \pm 0.5 \pm 0.3$	$1.4 \pm 0.1 \pm 0.1$
19	1.297	$6.1 \pm 0.6 \pm 0.6$	$1.8 \pm 0.1 \pm 0.1$
20	1.323	$6.7 \pm 0.6 \pm 0.5$	$1.7 \pm 0.1 \pm 0.1$
21	1.35	$7.0 \pm 0.8 \pm 0.6$	$1.8 \pm 0.1 \pm 0.2$
22	1.376	$7.5 \pm 0.8 \pm 0.7$	$2.0 \pm 0.1 \pm 0.1$
23	1.402	$9.2 \pm 1.0 \pm 0.9$	$2.1 \pm 0.1 \pm 0.1$
24	1.427	$9.1 \pm 1.0 \pm 0.9$	$2.3 \pm 0.1 \pm 0.2$
25	1.455	$9.1 \pm 1.0 \pm 1.6$	$2.6 \pm 0.1 \pm 0.1$
26	1.492	$7.0 \pm 0.9 \pm 1.1$	$3.1 \pm 0.1 \pm 0.2$
27	1.557	$2.3 \pm 0.5 \pm 0.7$	$4.3 \pm 0.2 \pm 0.4$
28	1.64	$2.8 \pm 1.1 \pm 1.3$	$4.7 \pm 0.3 \pm 0.7$
29	1.735	$3.1 \pm 1.1 \pm 2.3$	$6.0 \pm 0.5 \pm 1.4$

The fit projections are obtained by generating a large number of phase space MC events [15], weighting by the fit likelihood function, and normalizing the weighted sum to the observed number of events. There is good agreement between data and fit projections. Further tests of the fit quality are performed using unnormalized Y^0_L moment projections onto the $\pi^+\pi^-$ axis as functions of the helicity angle θ, which is defined as the angle between the π^- and the D^+_s in the $\pi^+\pi^-$ rest frame (or π^+ for D^-_s) (two combinations per event). The $\pi^+\pi^-$ mass distribution is then weighted by the spherical harmonic $Y^0_L(\cos\theta)$ ($L = 1 - 6$). The resulting distributions of the $\langle Y^0_L \rangle$ are shown in Fig. 4. A straightforward interpretation of these distributions is difficult, due to reflections originating from the symmetrization. However, the squares of the spin amplitudes appear in even moments, while interference terms appear in odd moments.

The fit produces a good representation of the data for all projections. The fit χ^2 is computed by dividing the Dalitz plot into 30×30 cells with 422 cells having entries. We obtain $\chi^2/NDF = 437/(422 - 64) = 1.2$. The χ^2 is also calculated using an adaptive binning with an average number of events per cell $\simeq 35$ [$\chi^2/NDF = 365/(391 - 64) = 1.1$], obtaining a χ^2 probability of 7.2%.

Attempts to include other resonant contributions, such as $\omega(782)$ or $f'_2(1525)$, do not improve the fit quality. MC simulations have been performed in order to validate the method and test for possible multiple solutions.

The results from the Dalitz plot analysis can be summarized as follows:

(i) The decay is dominated by the $D^+_s \to (\pi^+\pi^-)_{\mathcal{S}\ \rm wave}\pi^+$ contribution.

(ii) The $\mathcal{S}$ wave shows, in both amplitude and phase, the expected behavior for the $f_0(980)$ resonance.

(iii) The $\mathcal{S}$ wave shows further activity, in both amplitude and phase, in the regions of the $f_0(1370)$ and $f_0(1500)$ resonances.

(iv) The $\mathcal{S}$ wave is small in the $f_0(600)$ region, indicating that this resonance has a small coupling to $s\bar{s}$.

(v) There is an important contribution from $D^+_s \to f_2(1270)\pi^+$ whose size is in agreement with that reported by FOCUS, but a factor of 2 smaller than that reported by E791. This is the largest contribution in charm decays from a spin-2 resonance.

(vi) We observe a similar trend for the $\mathcal{S}$ wave amplitude and phase among the three experiments. Our results agree better (within uncertainties) with the results from FOCUS than those from E791.

Our results may be compared with different measurements of the $\pi\pi$ amplitude and phase from many other sources. For a recent review, see [16].

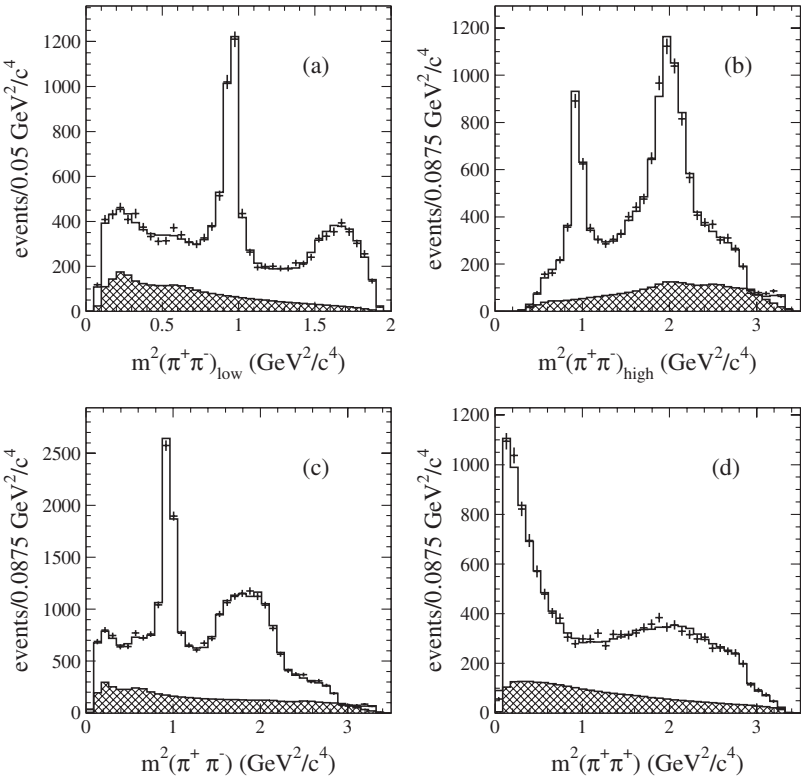

FIG. 3. Dalitz plot projections (points with error bars) and fit results (solid histogram). (a) $m^2(\pi^+\pi^-)_{\rm low}$, (b) $m^2(\pi^+\pi^-)_{\rm high}$, (c) total $m^2(\pi^+\pi^-)$, and (d) $m^2(\pi^+\pi^+)$. The hatched histograms show the background distribution.

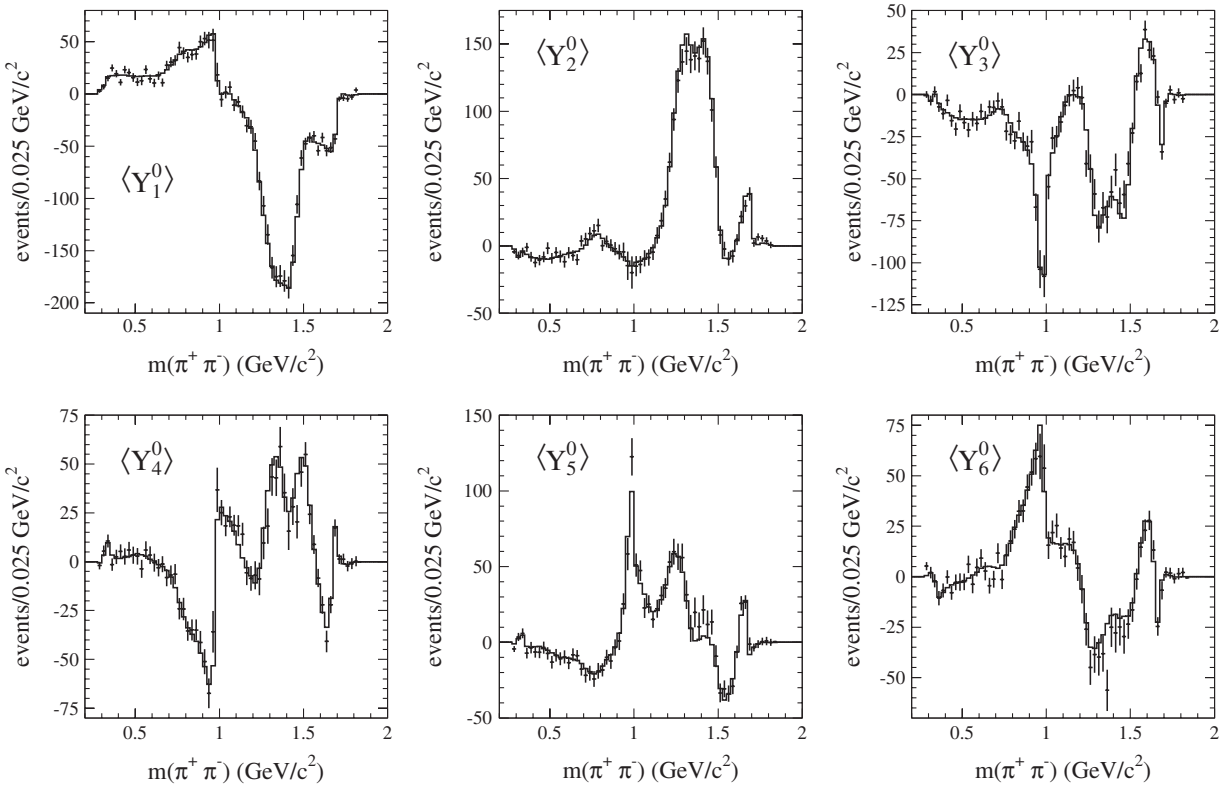

FIG. 4. Unnormalized spherical harmonic moments $\langle Y_L^0 \rangle$ as a function of $\pi^+\pi^-$ effective mass. The data are presented with error bars, and the histograms represent the fit projections.

Systematic uncertainties on the fitted fractions are evaluated in different ways:

(i) The background parametrization is performed using the information from the lower/higher sideband only or both sidebands.
(ii) The Blatt-Weisskopf barrier factors have a single parameter r which we take to be 1.5 $(\mathrm{GeV}/c)^{-1}$ and which has been varied between 0 and 3 $(\mathrm{GeV}/c)^{-1}$.
(iii) Results from fits which give equivalent Dalitz plot descriptions and similar sums of fractions (but worse likelihood) are considered.
(iv) The likelihood cut is relaxed but the mass cut on the $\pi^+\pi^-\pi^+$ is narrowed in order to obtain a similar purity.
(v) The purity of the signal, the resonance parameters and the efficiency coefficients are varied within their statistical errors.
(vi) The $\rho(770)$ and $\rho(1450)$ parametrization is modified according to the Gounaris-Sakurai model [17].
(vii) The number of steps used to describe the $\mathcal{S}$ wave has been varied by ± 2.

VII. BRANCHING FRACTION

Since the two D_s^+ decay channels (1) and (3) have similar topologies, the ratio of branching fractions is expected to have a reduced systematic uncertainty. We therefore select events from the two D_s^+ decay modes using similar selection criteria for the D_s^{*+} selection and for the likelihood test. For this measurement, a looser likelihood cut is used.

The ratio of branching fractions is evaluated as

$$\mathrm{BR} = \frac{\sum_{x,y} \frac{N_1(x,y)}{\epsilon_1(x,y)}}{\sum_{x,y} \frac{N_0(x,y)}{\epsilon_0(x,y)}}, \tag{8}$$

where $N_i(x, y)$ represents the number of events measured for channel i, and $\epsilon_i(x, y)$ is the corresponding efficiency in a given Dalitz plot cell (x, y). For this calculation each Dalitz plot was divided into 50×50 cells.

To obtain the yields and measure the relative branching fractions, the $\pi^+\pi^-\pi^+$ and $K^+K^-\pi^+$ mass distributions are fit assuming a double Gaussian signal and linear background where all the parameters are floated. Systematic uncertainties, summarized in Table III, take into account uncertainties from MC statistics and from the selection criteria used.

The resulting ratio is

$$\frac{\mathcal{B}(D_s^+ \to \pi^+\pi^-\pi^+)}{\mathcal{B}(D_s^+ \to K^+K^-\pi^+)} = 0.199 \pm 0.004 \pm 0.009 \tag{9}$$

consistent, within 1 standard deviation, with the Particle Data Group [12] value: $0.265 \pm 0.041 \pm 0.031$. It is also consistent with a recent measurement from CLEO [18]: $0.202 \pm 0.011 \pm 0.009$.

TABLE III. Summary of systematic uncertainties on the $\mathcal{B}(D_s^+ \to \pi^+\pi^-\pi^+)/\mathcal{B}(D_s^+ \to K^+K^-\pi^+)$ ratio.

Source	Systematic uncertainties (%)
MC statistics	0.9
Δm cut	1.5
Likelihood cut	2.6
Particle identification	3.0
Total	4.3

The study of the $D_s^+ \to K^+K^-\pi^+$ decay can give new information on the $K\bar{K}$ $\mathcal{S}$ wave. This information together with the results reported in this analysis will enable new measurements of the $f_0(980)$ couplings to $\pi\pi/K\bar{K}$.

VIII. CONCLUSIONS

A Dalitz plot analysis of approximately 13 000 $D_s^+ \to \pi^+\pi^-\pi^+$ has been performed. The fit measures fractions and phases for quasi-two-body decay modes. The amplitude and phase of the $\pi^+\pi^-$ $\mathcal{S}$ wave is extracted in a model-independent way for the first time. We also measure with high precision the $\mathcal{B}(D_s^+ \to \pi^+\pi^-\pi^+)/\mathcal{B}(D_s^+ \to K^+K^-\pi^+)$ ratio.

ACKNOWLEDGMENTS

We are grateful for the extraordinary contributions of our PEP-II colleagues in achieving the excellent luminosity and machine conditions that have made this work possible. The success of this project also relies critically on the expertise and dedication of the computing organizations that support *BABAR*. The collaborating institutions wish to thank SLAC for its support and the kind hospitality extended to them. This work is supported by the U.S. Department of Energy and National Science Foundation, the Natural Sciences and Engineering Research Council (Canada), the Commissariat à l'Energie Atomique and Institut National de Physique Nucléaire et de Physique des Particules (France), the Bundesministerium für Bildung und Forschung and Deutsche Forschungsgemeinschaft (Germany), the Istituto Nazionale di Fisica Nucleare (Italy), the Foundation for Fundamental Research on Matter (The Netherlands), the Research Council of Norway, the Ministry of Education and Science of the Russian Federation, Ministerio de Educación y Ciencia (Spain), and the Science and Technology Facilities Council (United Kingdom). Individuals have received support from the Marie-Curie IEF program (European Union) and the A. P. Sloan Foundation.

[1] M. Bauer, B. Stech, and M. Wirbel, Z. Phys. C **34**, 103 (1987).
[2] E. M. Aitala *et al.* (E791 Collaboration), Phys. Rev. Lett. **89**, 121801 (2002); **86**, 770 (2001).
[3] See for example F. E. Close and N. A. Tornqvist, J. Phys. G **28**, R249 (2002).
[4] All references in this paper to an explicit decay mode imply the use of the charge conjugate decay also.
[5] E. M. Aitala *et al.* (E791 Collaboration), Phys. Rev. D **73**, 032004 (2006).
[6] E. M. Aitala *et al.* (E791 Collaboration), Phys. Rev. Lett. **86**, 765 (2001).
[7] J. M. Link *et al.* (FOCUS Collaboration), Phys. Lett. B **585**, 200 (2004).
[8] B. Aubert *et al.* (*BABAR* Collaboration), Nucl. Instrum. Methods Phys. Res., Sect. A **479**, 1 (2002).
[9] T. Sjostrand, S. Mrenna, and P. Skands, J. High Energy Phys. 05 (2006) 026.
[10] S. Agostinelli *et al.* (GEANT4 Collaboration), Nucl. Instrum. Methods Phys. Res., Sect. A **506**, 250 (2003).
[11] P. Golonka *et al.*, Comput. Phys. Commun. **174**, 818 (2006).
[12] W. M. Yao *et al.*, J. Phys. G **33**, 1 (2006), and 2007 partial update for 2008.
[13] J. M. Blatt and V. F. Weisskopf, *Theoretical Nuclear Physics* (Wiley, New York, 1952).
[14] K. S. Kölbig and H. Lipps, CERN Program Library, Report No. E211.
[15] F. James, CERN Program Library, Report No. W515.
[16] E. Klempt and A. Zaitsev, Phys. Rep. **454**, 1 (2007).
[17] G. J. Gounaris and J. J. Sakurai, Phys. Rev. Lett. **21**, 244 (1968).
[18] J. P. Alexander *et al.* (CLEO Collaboration), Phys. Rev. Lett. **100**, 161804 (2008).